Friction models of kink-banding in compressed layered structures

G. W. Hunt
Department of Mechanical Engineering, University of Bath, UK
M. Ahmer Wadee
Department of Civil & Environmental Engineering, Imperial College, London, UK
M. A. Peletier
Centrum voor Wiskunde en Informatica, Amsterdam, the Netherlands

ABSTRACT: An earlier prototype model for kink-banding in constrained layered structures, compressed in a layer-parallel direction, is summarized and extended. Important ingredients include layer-parallel stiffness, interlayer friction, overburden pressure and layer bending stiffness. The Maxwell stability criterion is proposed as a useful lower bound for failure loads and displacements. Predictions of angle of rotation, band orientation across the layers, kink band width, and initiation and propagation loads, are compared with simple preliminary small scale experiments on confined specimens comprising layers of paper.

1 INTRODUCTION

Kink banding in layered and fibrous structures under layer-parallel compression is a thoroughly nonlinear phenomenon with manifestations throughout the physical sciences. Examples include deformation of geological strata (Anderson 1964; Hobbs et al. 1976), wood compressed along its grain (Reid & Peng 1997), compressed fibre composites (Hull & Clyne 1996; Fleck 1997), and internal kinking of wound cables (Hobbs et al. 1995). An earlier paper (Hunt et al. 2000) modelled the geological appearance of kink banding in stratified layers confined by overburden pressure and under slow tectonic compression (interpreted as prescribed end-shortening). Significant effects were found to be linked to the initial in-plane stiffness, inter-layer friction, and penalization of void formation. The resulting model reproduced the qualitative response with some success, but quantitative prediction was at that time considered to be beyond its immediate scope.

Here we attempt to overcome these limitations. The earlier model required the width of the kink band to be chosen a priori, but with the simple addition of a term to represent strain energy of bending in the layers, this restriction can be relaxed. The compromise between energy absorbed in friction and in bending gives a natural length scale to the instability, and the system is able to choose a finite band width according to a minimum energy criterion. Most importantly, this enables quantitative comparison between the model and simple experiments on confined layers of paper (see Fig. 1). Theoretical predictions for initiation and

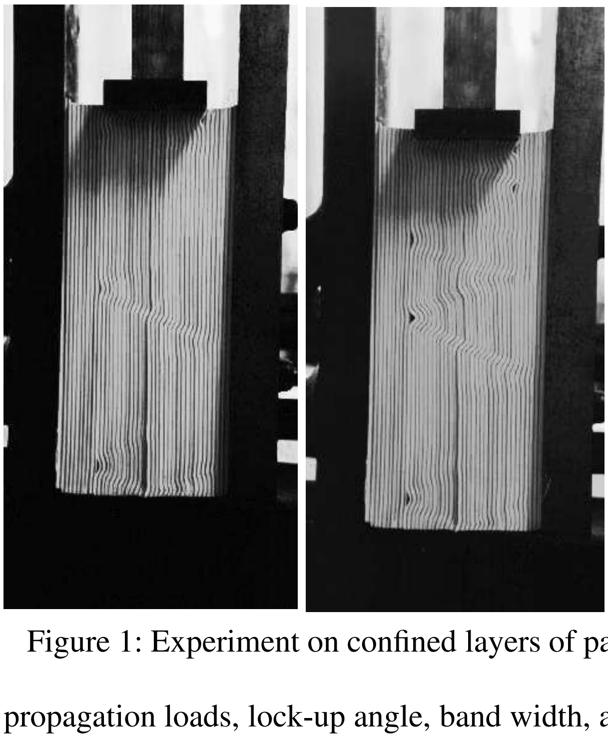

Figure 1: Experiment on confined layers of paper.

propagation loads, lock-up angle, band width, and its orientation, are thus made available for verification.

The frictional nature of the response of course suggests dissipation of energy, but for reasons that will become apparent we adopt an energy or virtual work approach. This presupposes that the displacement never reverses and hysteresis is never called into play. The formulation thus cannot distinguish between dissipative and non-dissipative constitutive laws, and the equilibrium states of one must coincide with those of the other.

2 PROTOTYPE MODEL

The prototype models of (Hunt et al. 2000) represented kink banding by a stack of rigid blocks of width b, confined by an overburden pressure q, and with a layer-parallel stiffness k (see Fig. 2a). A key

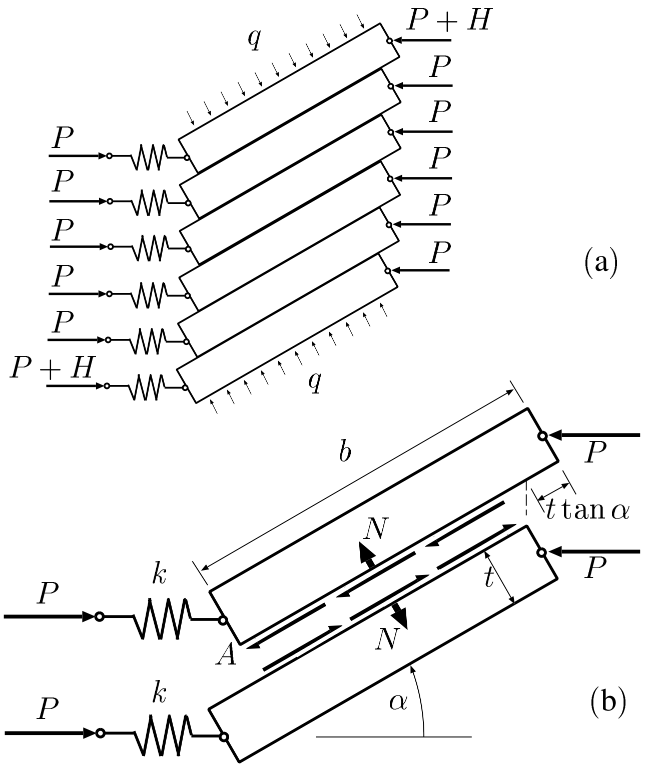

Figure 2: Full stack of blocks and representative two-layer section.

element was the sliding friction between the layers, which was modelled by a simple Coulomb friction law with coefficient μ. A representative section of two layers is shown in Figure 2b. Two configurations were considered, the vertical stacking shown in Figure 2, which necessarily expands vertically and thus does work against overburden pressure q, and inclined stacking, where the stacking angle complies with the rotation, such that voids are denied and no direct work is done against q (See Fig. 3). In this latter case, q en-

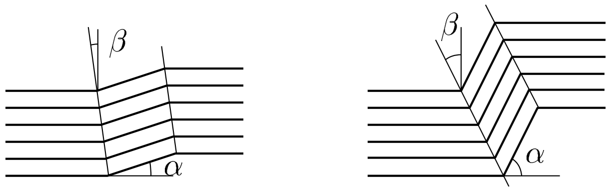

Figure 3: If no voids are to form, α must always equate to 2β.

ters the equation only via the friction term.

We now add to this formulation elastic rotational springs of stiffness c at the pin positions to represent the bending stiffness of the layers, using the vertical stack configuration as an illustration. In a general state represented by rotation α, band width b, and spring compression δ, the total potential energy function per layer of thickness t is

$$V = \frac{1}{2}k\delta^2 + c\alpha^2 - qbt\ln(\cos\alpha - \mu\sin\alpha)$$
$$-P[\delta + b(1-\cos\alpha)] \qquad (1)$$

where the first term is the energy stored in in-plane compression, the second is the strain energy stored in the two rotational springs, the third is the combination of work done against friction and overburden pressure, and the final term is the work done by the load P. Partial differentiation with respect to the three degrees of freedom α, δ and b produces three equilibrium equations, identical to those obtained from a virtual work formulation in which, in the general configuration, incremental virtual displacements are introduced in the three variables. Introducing the transformation

$$\delta = t\tilde{\delta}, \quad b = t\tilde{b}, \quad q = k\tilde{q}, \quad c = kt^2\tilde{c}, \quad P = kt\tilde{p} \qquad (2)$$

and immediately dropping the tildes leads to the non-dimensionalized form for V,

$$V = \frac{1}{2}\delta^2 + c\alpha^2 - qb\ln(\cos\alpha - \mu\sin\alpha)$$
$$-p[\delta + b(1-\cos\alpha)] \qquad (3)$$

The three equilibrium equations $\partial V/\partial\alpha = 0$, $\partial V/\partial\delta = 0$ and $\partial V/\partial b = 0$ produce two distinct solutions, which can be written

either: $\alpha = 0,\ p = \delta,$ with b indeterminate $\qquad (4)$

$$\text{or: } p = \delta = \frac{2c\alpha}{b\sin\alpha} + \frac{q}{\sin\alpha}\left(\frac{\mu + \tan\alpha}{1 - \mu\tan\alpha}\right)$$
$$= -\frac{q\ln(\cos\alpha - \mu\sin\alpha)}{1-\cos\alpha} \qquad (5)$$

Elimination of p gives an explicit form for the kink band width b in terms of c, q and α

$$b = 2c\alpha\left[(\cos\alpha - 1)(1-\mu\tan\alpha)\right]/R,$$

$$\text{where } R = q\left[\sin\alpha(1-\mu\tan\alpha)\ln(\cos\alpha - \mu\sin\alpha)\right.$$
$$\left.+(1-\cos\alpha)(\mu+\tan\alpha)\right] \qquad (6)$$

Figure 4 shows both solutions on a plot of load p against total end shortening $\Delta = \delta + b(1-\cos\alpha)$.

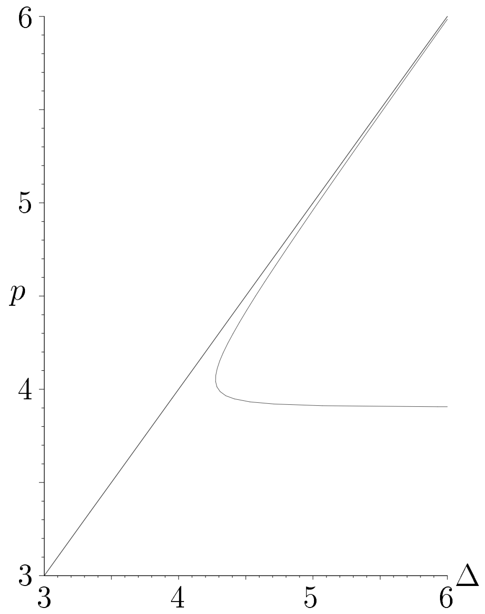

Figure 4: Equilibrium response of vertical stack model.

The linear pre-buckling solution (4) and nonlinear post-buckling solution (5) approach one another asymptotically as $p \to \infty$ but never meet. Thus, for incrementally-small displacements away from the pre-buckled state, there is no adjacent position of equilibrium, and no bifurcation points exist on the pre-buckled path. Not only does this suggest, erroneously, that the system can maintain stability up to infinite load, but the usual practices of linearization can now serve no useful purpose.

2.1 *Inclined stacking*

A similar modelling process for the inclined stack configuration generates the potential function (Wadee et al. 2000)

$$V = \frac{1}{2}\delta^2 + c\alpha^2 + \frac{\mu q b}{2}\int_0^\alpha \frac{\sec^2(\alpha'/2)\mathrm{d}\alpha'}{(1-\mu\tan\alpha')} - p\delta - (p-q)b(1-\cos\alpha) \qquad (7)$$

leading to the equilibrium equations

$$\frac{p}{q} = \frac{\delta}{q} = 1 + \frac{\mu}{\sin\alpha(1+\cos\alpha)(1-\mu\tan\alpha)} + \frac{2c\alpha}{qb\sin\alpha} = 1 + \frac{\mu}{2(1-\cos\alpha)}\int_0^\alpha \frac{\sec^2(\alpha'/2)\mathrm{d}\alpha'}{(1-\mu\tan\alpha')} \qquad (8)$$

replacing equation (5) for the post-buckling curve. This gives the expression

$$b = \frac{2c\alpha}{\mu q}\left[\frac{\sin\alpha}{2(1-\cos\alpha)}\int_0^\alpha \frac{\sec^2(\alpha'/2)\mathrm{d}\alpha'}{(1-\mu\tan\alpha')} - \frac{1}{(1+\cos\alpha)(1-\mu\tan\alpha)}\right]^{-1} \qquad (9)$$

for the band width. The two equilibrium solutions for the inclined stack configuration are shown in Figure 5. The form is the same as that of Figure 4 for the

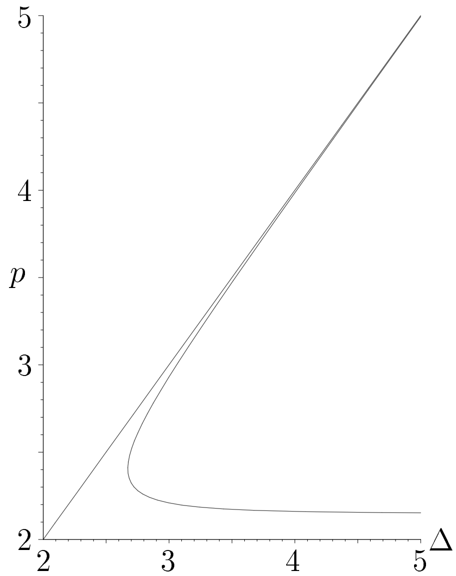

Figure 5: Equilibrium response of inclined stack model.

vertical stack but with loads that are generally lower, indicating that the inclined stack is the preferred, least energy, solution.

2.2 *Maxwell criterion*

The characteristic form of Figures 4 and 5, although not uncommon in problems of localized buckling, presents an analytical conundrum. At high loads the pre-buckled state is liable to be one of advanced meta-stability, such that the slightest disturbance would trigger formation of the first band, yet there remains no bifurcation point from which to initiate the response analytically; on linearizing the equation, all evidence of the instability disappears. To offset this, we shall use as a basis for comparison with experiments the Maxwell Stability Criterion, where stability lies only with the global, as opposed to local, minima of energy. For a system with the form of Figure 6, for example, work done in displacement is numerically equal to the area under the curve in question. Under the Maxwell criterion and control of end-shortening Δ, the linear pre-buckling path becomes unstable when area A_1 is numerically equal to area A_2, whereupon a jump takes place to the lower part of nonlinear post-buckling curve. In the presence of underlying external disturbance, the Maxwell displacement Δ_M thus defined acts as a natural lower bound on the actual point of instability. No instability would be expected before $\Delta = \Delta_M$, and, depending on the magnitude of the underlying disturbances, stability of

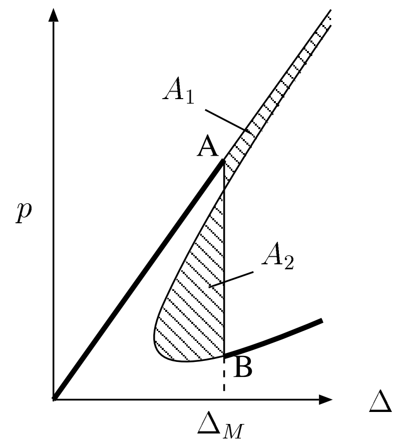

Figure 6: Maxwell stability criterion. When $A_1 = A_2$ the system will jump from A to B.

the pre-buckling state might hold for some way beyond it. Nevertheless, it does provide some, as opposed to no, basis for comparison with experiment. Numerically, $\Delta = \Delta_M$ when

$$\text{Area} = \int_{\alpha=0}^{\alpha=\alpha_M} (p - \Delta)\mathrm{d}\Delta = 0 \tag{10}$$

where α_M refers to the advanced post-buckled state, indicated by B.

2.3 *Mechanisms for propagation*

The Maxwell criterion gives a lower bound Δ_M on the critical end shortening for the initial instability, associated with the formation of a single kink band. Additional end shortening Δ must then lead to some form of propagation. This could be one of at least two different forms: either the band width could remain constant and bands propagate in zigzag fashion along the length (see Fig. 1), or the band width could grow. The earlier studies took band width b to be constant and so only first would apply, but for the present study either mechanism is possible.

In this respect, we note that Figures 4 and 5 contrast sharply with their counterparts from the earlier study (Hunt et al. 2000), in that in the advanced post-buckling regime, instead of passing through a minimum and emerging with positive stiffness, p remains relatively constant as both α and b grow with Δ. This mechanism is thus apparently less stiff than when b is fixed and therefore might seem the preferred option, but several simplifications need to be borne in mind. Most importantly, the variable b response is effectively formulated across an infinite specimen width; it does not account for doubling the end-shortening for example, when a band reflects from one side of the specimen or the other to create the zigzag pattern. Moreover, growth of b implies migration of hinge lines, for which in reality we would expect some kind of energy penalty; for the present model no such penalty applies, the energy required to deform one rotational elastic spring being always offset by that released in the undoing of another. A comparative energy study of the two propagation models, including hinge migration and the strong coupling between adjacent bands that must occur at the corners of the zigzag pattern, remains a possibility that at present is beyond our capability.

Both mechanisms are apparently active however, in the sequence of photographs reported in (Hunt et al. 2000). First, an initial instability at some point of applied displacement, $\Delta > \Delta_M$, induces a single kink band to form across the width of the specimen. Strong coupling effects at the edges then promote second and subsequent bands form in zigzag fashion along the complete length, without noticeable growth in band width. Once complete, hinge lines start to migrate, continuing until the recognizable form of chevron folding, based on the wavelength of the initial zigzag pattern, is observed. Once the chevrons have formed completely, restabilization is complete, and the system finds itself thoroughly locked into the deformed state.

3 PARAMETERS FOR COMPARISON

The experimental configuration of interest is shown in diagrammatic form in Figure 7. Layers of paper are

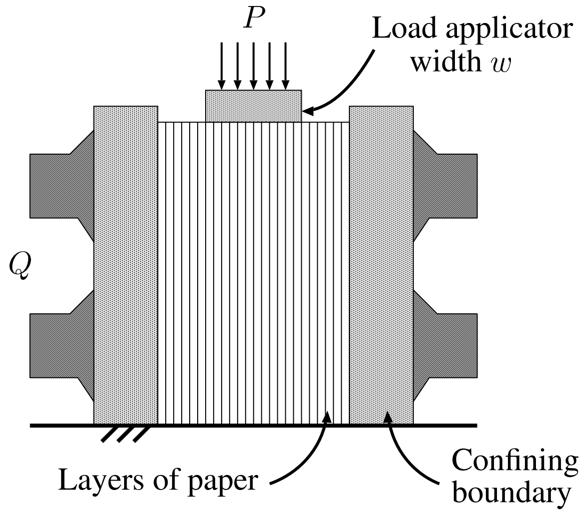

Figure 7: Experimental set up.

clamped laterally with force Q to simulate overburden pressure q, and compressed longitudinally under controlled end- shortening Δ in a 1 tonne Instron testing machine. Output to an x–y plotter gives the corresponding relationship between the load (P) and its corresponding deflection (Δ). This type of confined test has been performed in the past on stratified rocks (see for example (Paterson & Weiss 1966)).

The central plug under the load applicator, within which the kink bands form (see Fig. 1), is confined by overburden pressure and restricted by friction along its sides. To enable comparison with theory, parameters requiring evaluation include in-line stiffness (k), coefficient of friction for paper on paper (μ), constraining pressure (q) and bending stiffness of a single layer (represented by c). Typical output from the x–y plotter is shown in Figure 8. After the initial peak

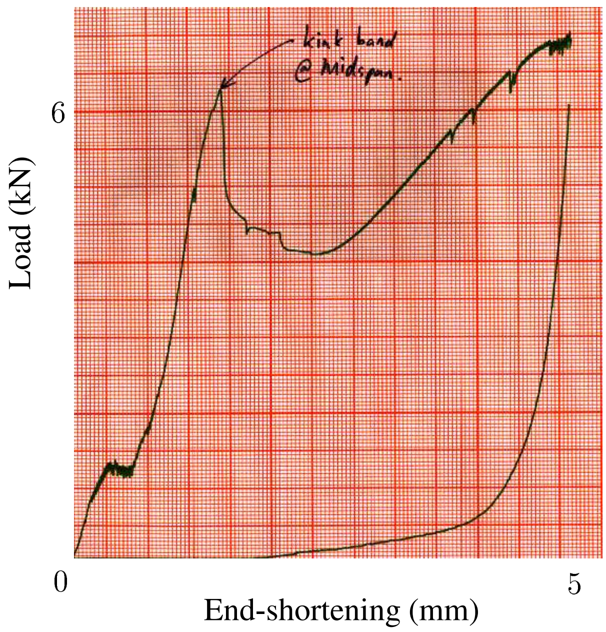

Figure 8: Typical output of x–y plotter.

load the response shows a sudden instability, marked by an instantaneous drop in load as the first kink band forms. This is followed by a further slight decrease, followed by restabilization and subsequent increase in load as bands propagating in zigzag fashion throughout the specimen, as discussed above, sometimes marked by small discontinuities or dips in the response. Once the zigzag pattern is fully developed, the stiffness of the response is found to be of the same order as that of the original flat state. As well as providing load levels to check against theory, other useful experimental output for checking includes kink band angle (α), orientation across the width (β), and band width (b).

3.1 *In-line stiffness and friction coefficient*

The in-line stiffness, k, of a single layer of paper can be estimated from the initial slope of the loading path of Figure 8, simply by dividing by the number of layers under the applicator. The coefficient of friction between layers of the selected paper is similarly easy to estimate, by conducting friction angle tests off an inclined plane. Of the order of twenty such tests were performed, under different weights to allow differences in reactive forces, with a reasonable degree of consistency. Typically, the friction angle varied between 28° and 32°. An average value of 30° was therefore taken for all comparisons, giving a coefficient of friction of $\mu = \tan \pi/6 = 0.58$.

3.2 *Overburden pressure*

Overburden pressure q can estimated directly from lateral pressure tests conducted in the same 1 tonne Instron testing machine, typically giving output as in Figure 9. Careful measurement of inwards lateral dis-

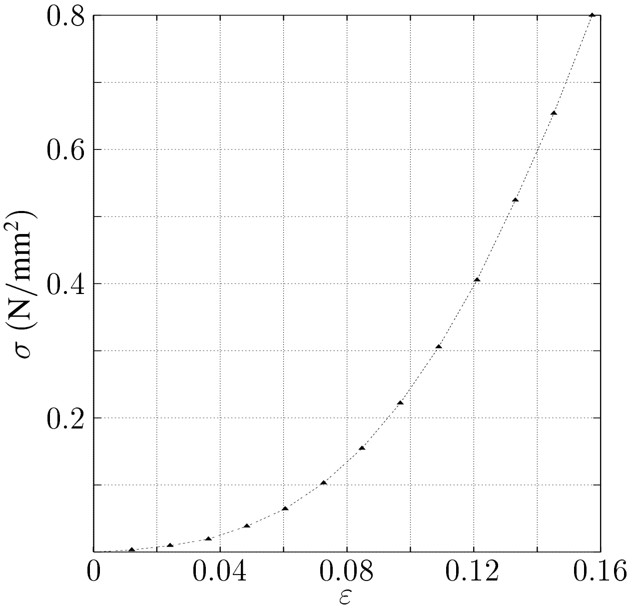

Figure 9: Lateral compression characteristics of test paper: compressive stress against compressive strain.

placement during the clamping process gives an estimate of compressive strain, which can be reinterpreted as compressive stress and thus initial overburden pressure by reading directly from the graph. The force Q shown in Figure 7 relates to the stress σ, and displacement z relates to the strain ε respectively: $\sigma = Q/A_{\text{paper}} = Q/(a_1 a_2)$ and $\varepsilon = z/a_3$, where a_1 and a_2 are the breadth (106 mm) and length (148 mm) of the sheets of paper respectively and a_3 is the initial sample width; as q is defined as a force per unit length, $q = \sigma a_1$. No attempt is made to account for changes in q during testing.

3.3 *Bending stiffness*

Estimates of bending energy are more difficult to obtain. The above model assumes all such energy is stored in elastic rotational springs of stiffness c, while close-up examination of a kink band corner reveals it to be sharp but curved; it is also noticeable that the greater the overburden pressure, the sharper the corner. With the object of determining the corresponding bending energy and replacing it with an equivalent rotational stiffness c, we next revisit a significant analytical development described in the Appendix of our earlier paper (Hunt et al. 2000).

The modelling was based on the observation that to avoid the formation of voids, a layered system would select straight limbs and sharp corners. This is because identical curved layers cannot be made to fit together snugly without creating voids while, subject to the constraint described in Figure 3, folded layers can. Simple bending theory tells us that the tighter the curve, the more energy is stored for the same overall change in angle, and so in the true situation a minimum energy balance must be struck between work done in bending and against overburden pressure.

The procedure involves fitting two identically-curved layers together as snugly as possible by optimizing their relative spatial positions, and integrating over the curve the resulting difference between the distance between the centrelines and the layer thickness, to produce the void area for the section. For a corner of total angle α, the associated energy is obtained by minimizing

$$J = \frac{D}{t}\left\{\frac{1}{2}\int_{-\infty}^{\infty}\theta'(s)^2\,\mathrm{d}s + \frac{qt^3}{D}\int_{-\infty}^{\infty} f(\theta)\,\mathrm{d}s\right\}$$

where the independent variable s measures non-dimensional arc length, $D = Et^3a_1/12$ is the cylindrical bending stiffness for a single layer of thickness t, E is Young's modulus, $f(\theta) = (\kappa\sin\theta(s) + \cos\theta(s) - 1)_+$, and $\kappa = \tan\alpha/2$. The first term represents the strain energy of bending of a single layer and the second is the work done in opening the void. The minimization is performed over all profiles $\theta : \mathbb{R} \to \mathbb{R}$ such that $\theta \to 0$ as $s \to -\infty$ and $\theta \to \alpha$ as $s \to \infty$, so both the shape and tightness of the curve are defined by this procedure.

We now use some of the results of (Hunt et al. 2000) to approximate J. It was shown that the minimal energy profile θ has a finite length, i.e. that there exists $s_h > 0$ such that $\theta \equiv \alpha$ if $s \geq s_h$ and $\theta \equiv 0$ if $s \leq s_h$. With the notation $\lambda^2 = qt^3/D$, it was also shown that $s_h \sim \lambda\pi/2$, approximately independently of α.

With this in mind we approximate the optimal profile by

$$\tilde{\theta}(s) = \begin{cases} 0 & s \leq -\lambda\pi/2 \\ \frac{\alpha}{2}(1+\sin s/\lambda) & -\lambda\pi/2 < s < \lambda\pi/2 \\ \alpha & s \geq \lambda\pi/2 \end{cases} \tag{11}$$

and approximate $f(\theta)$ by $\tilde{f}(\theta) = \frac{\kappa}{\alpha}\theta(\alpha - \theta)$. Thus we obtain the estimate

$$J \sim \sqrt{Dqt}\left\{\frac{\pi\alpha^2}{16} + \frac{\pi\kappa\alpha}{8}\right\}$$

Taking into account that $\kappa = \tan\alpha/2$, we arrive at the final estimate

$$J \sim \frac{1}{2}c\alpha^2 \qquad \text{with} \qquad c = \frac{\pi}{4}\sqrt{Dqt} \tag{12}$$

4 COMPARISON WITH EXPERIMENTS

The experimental configuration of Figure 7 induces a central plug of the width of the load applicator to move downwards relative to the layers outside it. Under overburden pressure q and when friction is active along the slip planes, the load on the plug cross-section therefore reduces with depth x measured from the top of the sample, by an amount approximated by

$$F(x) = 2\mu\int_0^x q(\xi)\,\mathrm{d}\xi \tag{13}$$

If q is constant throughout, kink banding thus always starts at the top, and only after significant locking can it propagate down the specimen. We can offset this tendency by compressing laterally the top of the sample more than the bottom. For each of the following experiments, estimates for q are taken at the top, middle and bottom of the specimen, based on assumed linear variations of compressive strain with depth. These are obtained from averaged values based upon lateral compression tests (see Figure 9) in which the sample is compressed to the same relative strain throughout.

Table 1 details the lateral compression characteristics before commencement of loading, for six separate experimental configurations, together with estimates of in-line stiffness k based upon the pre-kinked experimental stiffness. Table 2 describes the resulting estimates for the overburden pressure q, and bending stiffness parameter c determined from Equation (12). The lower bound estimates for the bandwidth

Table 1: Experimental lateral strains, load applicator width w (mm) and individual layer stiffness k (N/mm).

Expt	Confining strains			w	k
	Bottom	Middle	Top		
1	0.096	0.116	0.136	11.9	33.1
2	0.101	0.127	0.151	12.7	34.6
3	0.069	0.099	0.129	12.7	16.6
4	0.066	0.099	0.127	12.0	24.2
5	0.063	0.091	0.121	12.0	20.0
6	0.066	0.093	0.119	12.0	38.7

Table 2: Nondimensional quantities of overburden pressure q and rotational spring stiffness c.

Expt	Bottom		Middle		Top	
	q	c	q	c	q	c
1	0.679	6.7	1.127	8.6	1.769	10.8
2	0.803	7.3	1.439	9.7	2.277	12.2
3	0.580	8.7	1.504	14.0	3.066	20.0
4	0.359	5.7	0.950	9.2	1.993	13.4
5	0.387	6.5	1.028	10.1	2.119	15.1
6	0.219	3.5	0.537	5.5	1.057	7.7

at the Maxwell displacement, b_M, obtained from the inclined stack model after the introduction of confining (q) and material (c, k) parameters, are compared against experimental values in Table 3. Table 4 gives the corresponding theoretical predicitions for kink band angle α at the Maxwell condition. Figure 10 compares the predicted upper and lower loads of the dynamic jump at the Maxwell condition (A and B of Figure 6) with experimental loads at the point of initial instability, after allowance has been made for losses through the depth due to friction according to Equation (13). Experimental results were recorded in detail only for the initial instability, so this experimental curve is really only of immediate significance for the first band to form.

Table 3: Comparisons between experimental bandwidths and Maxwell predictions (mm).

Expt	Bottom		Middle		Top	
	b_{expt}	b_M	b_{expt}	b_M	b_{expt}	b_M
1	4.8	1.39	2.9	1.32	2.2	1.28
2	5.0	1.34	3.1	1.27	2.6	1.24
3	5.1	1.85	3.1	1.69	2.1	1.61
4	5.6	1.69	3.7	1.53	2.6	1.44
5	5.4	1.83	3.8	1.65	2.8	1.56
6	5.8	1.45	4.0	1.39	2.8	1.30

Table 4: Maxwell values of kink band angle α_M (rad). Experimentally, α at lockup is of the order of 0.8 rad.

Expt	Bottom	Middle	Top
1	0.319	0.380	0.442
2	0.338	0.413	0.479
3	0.277	0.388	0.488
4	0.244	0.346	0.444
5	0.245	0.348	0.444
6	0.216	0.299	0.379

4.1 *Discussion*

In all cases apart from at the bottom of the sample for Experiments 1 and 2, the Maxwell condition is seen to predict lower values of load, band width b, and angle α, than found experimentally. This is as expected (Hunt et al. 2000). The initial loading path readily surpasses the Maxwell condition, and so jumps occur to larger b and α, at higher load values, than suggested by the lower bound approach. Although experimental results were not recorded in detail past the initial instability, it is reasonable to suppose for Experiments 1 and 2 that: (a) the first band forms at the top; and (b) total load increases significantly before bands form at the bottom. Thus the validity of the right-hand parts of the experimental curves of Figures 10a and b is highly questionable.

Indeed, comparisons between theory and experiment towards the bottom of the sample are less good

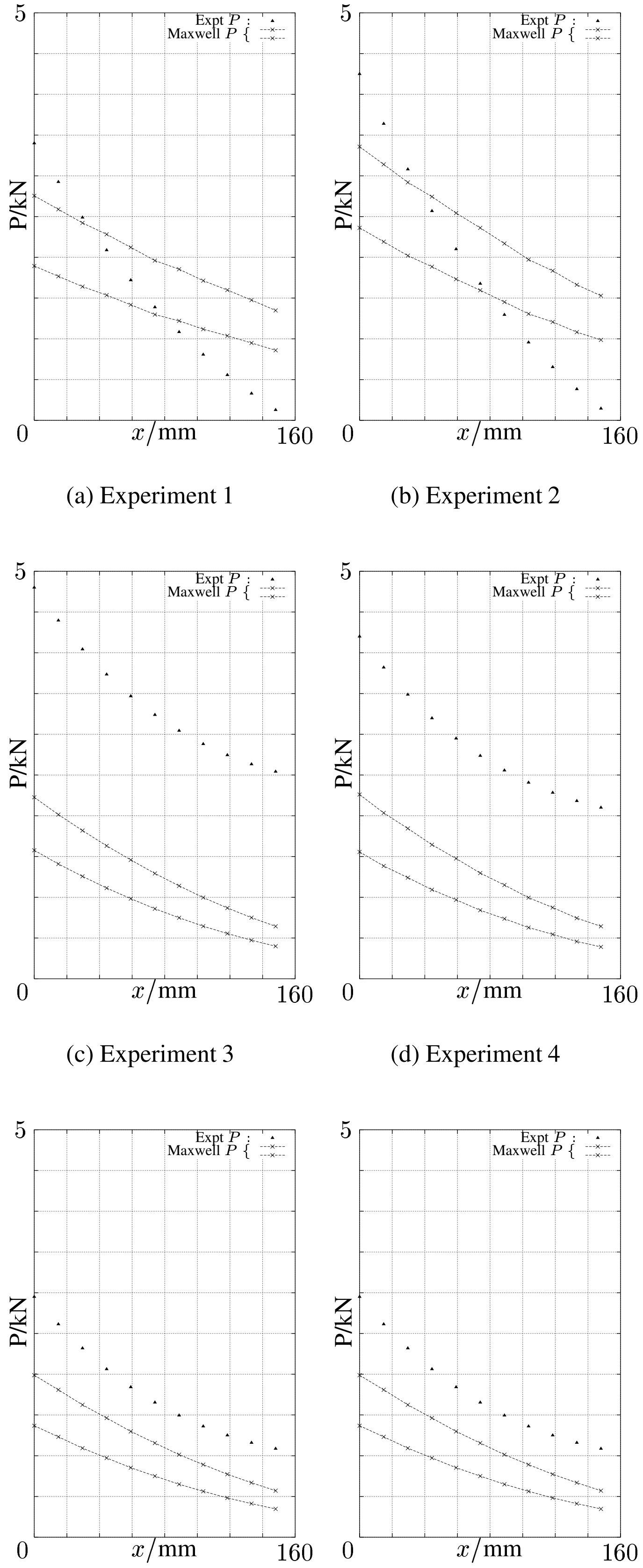

(a) Experiment 1 (b) Experiment 2

(c) Experiment 3 (d) Experiment 4

(e) Experiment 5 (f) Experiment 6

Figure 10: Upper and lower load values at the Maxwell condition, compared with experimental estimate at depth x.

for all experiments than those towards the top, at or near the position where the first band is likely to form. This is most apparent in the estimates for band width b seen in Table 3, and is worthy of some explanation. We put this effect down to the assumption that overburden pressure q is constant during the loading process. As the bottom bands tend form later, it is likely that the overburden pressure will have changed considerably by this stage in the loading history. The natural shearing movement associated with formation of the bands would be expected to influence the local value of q, as might the small triangular voids found at the corners of the zigzag pattern. In the present test configuration such effects are difficult to quantify. However, plans are underway for testing in a biaxial loading machine, with an ability to control and measure lateral loading independently of that applied longitudinally. Even then, local variations in q along the length may remain difficult to monitor.

5 CONCLUDING REMARKS

The paper represents our first attempt to model quantitatively the phenomenon of kink-banding in compressed and confined layered media, and clearly could benefit from refinement. Theoretical predictions for initial instability loads, angles of rotation α, and bandwidths b, are too low, as expected. Nevertheless, they are encouragingly of the right order in comparison with experiments, and always represent lower bounds on actual values, again as expected. For engineering purposes we might regard such Maxwell predictions as excessively low and thus unnaturally conservative, but geological conditions present quite different perspectives. Time scales are so long, possible underlying disturbances so strong, and associated uncertainties so profound, that any framework for quantitative prediction is likely to be useful. Maxwell conditions may well prove valuable in such circumstances.

The new contribution of this model compared with the earlier representation of (Hunt et al. 2000) is the addition of bending energy to the layers, represented simply by rotational elastic springs at the two extremes of the bandwidth. The single spring stiffness c representing this energy is developed from a more sophisticated minimum-energy formulation in which the layers pick up an optimum curved shape as they are fitted together. After the banded pattern is fully formed and the load is removed, fold lines are usually clearly visible in the paper. This suggests that plasticity is involved in the folding process, a fact that takes on greater significance once the migration of fold lines and consequent energy losses become an issue. Such considerations are beyond our immediate scope, although we certainly do not rule out some form of plastic analysis in future formulations. The essence of the nonlinear modelling process according to minimum energy principles, and its inherent adaptability, have nevertheless been fully demonstrated by this heuristic exercise.

REFERENCES

Anderson, T. B. (1964). Kink-bands and related geological structures. *Nature 202*, 272–274.

Fleck, N. A. (1997). Compressive failure of fiber composites. *Adv. Appl. Mech. 33*, 43–117.

Hobbs, B. E., Means, W. D., & Williams, P. F. (1976). *An Outline of Structural Geology*. New York: Wiley.

Hobbs, R. E., Overington, M. S., Hearle, J. W. S., & Banfield, S. J. (1995). Element buckling within ropes and cables. In *Proc. 2nd European Conf. on Flexible Pipes, Umbilicals and Marine Cables*, pp. 7.1–7.21. BPP Ltd.

Hull, D. & Clyne, T. W. (1996). *An introduction to composite materials* (2nd ed.). Cambridge Solid State Science Series. Cambridge University Press.

Hunt, G. W., Peletier, M. A., Champneys, A. R., Woods, P. D., Wadee, M. A., Budd, C. J., & Lord, G. J. (2000). Cellular buckling in long structures. *Nonlinear Dynamics 21*(1), 3–29.

Hunt, G. W., Peletier, M. A., & Wadee, M. A. (2000). The Maxwell stability criterion in pseudo-energy models of kink banding. *J. Structural Geology 22*, 667–679.

Paterson, M. S. & Weiss, L. E. (1966). Experimental deformation and folding in phyllite. *Bull. Geol. Soc. Am. 77*, 343–374.

Reid, S. R. & Peng, C. (1997). Dynamic uniaxial crushing of wood. *Int. J. Impact Engng. 19*, 531–570.

Wadee, M. A., Peletier, M. A., & Hunt, G. W. (2000). Maxwell stability criterion in models of kink banding: comparison with physical experiments. In preparation.